

Banner appropriate to article type will appear here in typeset article

Attenuation of turbulence in a periodic cube by finite-size spherical solid particles

Sunao Oka[†] and Susumu Goto[‡]

Graduate School of Engineering Science, Osaka University,
1-3 Machikaneyama, Toyonaka, Osaka, 560-8531 Japan

(Received xx; revised xx; accepted xx)

To investigate the attenuation of turbulence in a periodic cube due to the addition of spherical solid particles, we conduct direct numerical simulations using an immersed boundary method with resolving flow around each particle. Numerical results with systematically changing particle diameters and Stokes numbers for a fixed volume fraction show that the additional energy dissipation rate in the wake of particles determines the degree of the attenuation of turbulent kinetic energy. On the basis of this observation, we propose the formulae describing the condition and degree of the attenuation of turbulence intensity. We conclude that particles with the size proportional to $\lambda/\sqrt{\gamma}$, where λ and γ are the Taylor length and the mass density ratio between particles and fluid, most significantly reduce the intensity of developed turbulence.

Key words:

1. Introduction

We investigate solid particle suspension, where flow advects particles and vortices shedding from particles can change surrounding flow. Such fluid-particle interactions play essential roles in many flow systems. In particular, the enhancement and attenuation of turbulence by the addition of solid particles are important in industrial and environmental flows. However, there remain many unsolved scientific issues on the complex phenomena. In fact, although turbulence modulation due to solid particles is a classical issue in fluid mechanics back to the seminal experiments by [Tsuji & Morikawa \(1982\)](#) and [Tsuji *et al.* \(1984\)](#) about 40 years ago, there is no clear conclusion even for the most fundamental question: i.e. what determines the condition for the turbulence modulation? [Gore & Crowe \(1989\)](#) proposed a criterion on this issue by compiling the data of particulate turbulent pipe flow and jet. They concluded that turbulence was enhanced (or attenuated) if the ratio D/L , with D and L being the particle diameter and the integral

[†] Email address for correspondence: s_oka@fm.me.es.osaka-u.ac.jp

[‡] Email address for correspondence: s.goto.es@osaka-u.ac.jp

length [$L = 0.2 \times$ (pipe radius) for pipe flow and $0.039 \times$ (distance from the exit) for jet], is larger (or smaller) than 0.1 because larger particles produce turbulence in their wake, while smaller ones acquire their energy from large-scale vortices. Since then, even recently experiments with newer techniques such as particle tracking (Cisse *et al.* 2015) and particle image velocimetry (Hoque *et al.* 2016) were conducted. However, Gore & Crowe (1989)'s picture still holds, although Hoque *et al.* (2016), for example, proposed a more accurate estimation of the criterion of the enhancement and attenuation of homogeneous turbulence.

Numerical simulations have been playing important roles in the investigation of this complex phenomenon with many control parameters. Elghobashi & Truesdell (1993) and Elghobashi (1994) conducted numerical simulations of particulate turbulence. Their simulations were conducted with point-wise particles that obey the Maxey & Riley (1983) equation, and they showed the importance of the normalized particle velocity relaxation time (i.e. the Stokes number). Although continuum approaches (Crowe *et al.* 1996) were also used, we have to resolve flow around each particle to accurately treat fluid-particle interactions. Numerical methods for such direct numerical simulations (DNS) with finite size particles were proposed in this century (Kajishima *et al.* 2001; Ten Cate *et al.* 2004; Uhlmann 2005; Burton & Eaton 2005). For example, Kajishima *et al.* (2001) numerically demonstrated turbulence enhancement by finite-size particles. Since then, numerical schemes have been developing to more easily and accurately treat the non-slip boundary condition on particles' surface. Thanks to these developments, many authors recently conducted DNS of particulate turbulence under realistic boundary conditions: for example, channel flow (Uhlmann 2008; Shao *et al.* 2012; Picano *et al.* 2015; Wang *et al.* 2016; Fornari *et al.* 2016; Costa *et al.* 2016, 2018; Peng *et al.* 2019), pipe flow (Peng & Wang 2019), duct flow (Lin *et al.* 2017) and Couette flow (Wang *et al.* 2017).

In the present study, as a first step towards the complete clarification, prediction and control of the interaction between solid particles and turbulence, we examine the simplest case: namely, the modulation of turbulence by finite-size solid spherical particles in a periodic cube. Many authors (Ten Cate *et al.* 2004; Homann & Bec 2010; Lucci *et al.* 2010, 2011; Gao *et al.* 2013; Uhlmann & Chouippe 2017; Schneiders *et al.* 2017) numerically studied behaviors of finite-size particles in periodic turbulence. Concerning turbulent modulation, Ten Cate *et al.* (2004) conducted DNS of turbulence of particle suspension at the Taylor-length-based Reynolds number $R_\lambda = 61$ and demonstrated the enhancement of energy dissipation due to the excitation of particle-size flow. Lucci *et al.* (2010, 2011) showed by DNS with an immersed boundary method that turbulence modulation by finite-size particles were different from that caused by point-wise particles (Ferrante & Elghobashi 2003). More concretely, the decay rate of turbulence with the initial Reynolds numbers R_λ being between 25 and 110 is different depending on the particle size even if the Stokes number was identical. Gao *et al.* (2013) also examined this result by a different numerical method. Furthermore, recently, Schneiders *et al.* (2017) conducted very accurate DNS to investigate flow around Kolmogorov-scale particles in turbulence at moderate Reynolds number ($R_\lambda < 50$) and proposed the estimation of the energy dissipation rate around them. Although these previous studies provided with useful information on the turbulence modulation due to particle additives, the condition for the turbulence modulation (i.e. attenuation or enhancement) has not been clarified because of the lack of systematic parametric studies.

The present study aims at showing the condition for finite-size particles to attenuate turbulence. To this end, we conduct a systematic parametric study by means of DNS of forced turbulence in a periodic cube, and investigate turbulence modulation due to spherical solid particles with different diameters and Stokes numbers for a fixed volume fraction. Then, based on the obtained numerical results, we propose formulae that give the condition and degree of turbulence attenuation.

2. Direct numerical simulations

2.1. Numerical methods

The fluid velocity $\mathbf{u}(\mathbf{x}, t)$ at position \mathbf{x} and time t is governed by the Navier–Stokes equation,

$$\frac{\partial \mathbf{u}}{\partial t} + \mathbf{u} \cdot \nabla \mathbf{u} = -\frac{1}{\rho_f} \nabla p + \nu \nabla^2 \mathbf{u} + \mathbf{f} + \mathbf{f}^{\leftarrow p}, \quad (2.1)$$

and the continuity equation,

$$\nabla \cdot \mathbf{u} = 0, \quad (2.2)$$

for an incompressible fluid in a periodic cube with side $L_0 (= 2\pi)$. Here, $p(\mathbf{x}, t)$ is the pressure field, and ρ_f and ν denote the fluid mass density and kinematic viscosity, respectively. In (2.1), $\mathbf{f}^{\leftarrow p}(\mathbf{x}, t)$ is the force due to suspended solid spherical particles, whereas $\mathbf{f}(\mathbf{x}, t)$ is an external body force driving turbulence. In the present study, we examine the two cases with different kinds of external force $\mathbf{f}(\mathbf{x}, t)$. One is a time-independent forcing (Goto *et al.* 2017):

$$\mathbf{f}^{(v)} = (-\sin x \cos y, +\cos x \sin y, 0). \quad (2.3)$$

The other forcing $\mathbf{f}^{(i)}(\mathbf{x}, t)$ is a force which keeps the energy input rate P constant (Lamorgese *et al.* 2005). This forcing is concretely expressed in terms of its Fourier transform $\widehat{\mathbf{f}}^{(i)}(\mathbf{k}, t)$, where \mathbf{k} is the wavenumber, as

$$\widehat{\mathbf{f}}^{(i)}(\mathbf{k}, t) = \begin{cases} \frac{P}{2E_f(t)} \widehat{\mathbf{u}}(\mathbf{k}, t) & \text{if } 0 < |\mathbf{k}| \leq k_f, \\ 0 & \text{otherwise.} \end{cases} \quad (2.4)$$

In (2.4), $\widehat{\mathbf{u}}(\mathbf{k}, t)$ and E_f are the Fourier transform of $\mathbf{u}(\mathbf{x}, t)$ and the kinetic energy

$$E_f = \sum_{0 < |\mathbf{k}| \leq k_f} \frac{1}{2} |\widehat{\mathbf{u}}|^2 \quad (2.5)$$

in the forcing wavenumber range ($0 < |\mathbf{k}| \leq k_f$), respectively. We set $P = 1$ and $k_f = 1.5$. Note that $\mathbf{f}^{(i)}$ sustains statistically homogeneous isotropic turbulence, whereas $\mathbf{f}^{(v)}$ sustains turbulence with a mean flow.

In the present DNS, we use the second-order central finite difference on a staggered grid to estimate the spatial derivatives in (2.1). We use $N^3 = 256^3$ grid points for the main series of DNS, and 512^3 points for accuracy verifications. We summarize, in table 1, other numerical parameters and the statistics of the single-phase turbulence. In the present study, we estimate the integral length $L(t)$ by $3\pi \int_0^\infty k'E(k', t)dk'/4 \int_0^\infty E(k', t)dk'$, where $E(k, t)$ is the energy spectrum, and the Taylor length $\lambda(t)$ by $\sqrt{10\nu K'(t)/\epsilon(t)}$, where $\epsilon(t)$ is the spatial average of the

energy dissipation rate and $K'(t)$ is the turbulent kinetic energy:

$$K'(t) = \frac{1}{2} \left\langle \left| \mathbf{u}(\mathbf{x}, t) - \mathbf{U}(\mathbf{x}) \right|^2 \right\rangle \quad \text{with} \quad \mathbf{U}(\mathbf{x}) = \overline{\mathbf{u}(\mathbf{x}, t)}. \quad (2.6)$$

Here, $\langle \cdot \rangle$ and $\overline{\cdot}$ denote the spatial and temporal averages, respectively. Then, the Taylor-length-based Reynolds number is evaluated by $R_\lambda(t) = u'(t)\lambda(t)/\nu$, where $u'(t) = \sqrt{2K'(t)/3}$. We also estimate the Kolmogorov length by $\eta(t) = \epsilon(t)^{-1/4} \nu^{3/4}$.

We estimate the particle-fluid interaction force $\mathbf{f}^{\leftarrow p}(\mathbf{x}, t)$ in (2.1) by an immersed boundary method (Uhlmann 2005). In this method, we uniformly distribute N_L Lagrangian force points on each particle surfaces (Saff & Kuijlaars 1997; Lucci *et al.* 2010) to estimate the interaction force $\tilde{\mathbf{f}}^{\leftarrow p}$ by imposing the non-slip boundary condition of the fluid velocity on these points. The force $\mathbf{f}^{\leftarrow p}(\mathbf{x}, t)$ is determined by redistributing $\tilde{\mathbf{f}}^{\leftarrow p}$ onto grid points, whereas the force $\mathbf{f}_j^{\leftarrow f}$ and moment $\mathbf{L}_j^{\leftarrow f}$ around the particle center acting on the j th particle are estimated by integrating the reaction, $-\tilde{\mathbf{f}}^{\leftarrow p}$, on the particle's surface. Then, we obtain the position $\mathbf{x}_j(t)$, velocity $\mathbf{v}_j(t) = d\mathbf{x}_j/dt$ and angular velocity $\boldsymbol{\omega}_j(t)$ of the j th particle ($1 \leq j \leq N_p$ with N_p being the number of particles) by integrating Newton's equations of motion:

$$m \frac{d\mathbf{v}_j}{dt} = \mathbf{f}_j^{\leftarrow f} + \mathbf{f}_j^{\leftarrow p} \quad (2.7)$$

and

$$I \frac{d\boldsymbol{\omega}_j}{dt} = \mathbf{L}_j^{\leftarrow f}. \quad (2.8)$$

Here, we denote the diameter and mass density of the particles by D and ρ_p , and therefore the mass and inertial moment of a particle are $m = \pi\rho_p D^3/6$ and $I = mD^2/10$, respectively. In (2.7), $\mathbf{f}^{\leftarrow p}$ is the interaction force between particles. For this, we only consider the normal force due to the elastic collisions of particles. We have also neglected the gravity.

We numerically integrate the equations of motions (2.1), (2.7) and (2.8) by the fractional step method (Uhlmann 2005), where we use the second-order Adams-Bashforth method instead of the three-step Runge-Kutta method. We integrate the viscous term in (2.1) by the second-order Crank-Nicolson method and the elastic force in (2.7) by the first-order Euler method. The Poisson equation for the pseudo-pressure and the Helmholtz equation for the implicit integration of the viscous term are solved by using the fast Fourier transform.

2.2. Parameters

For a given external forcing, the parameters of fluid phase are the kinematic viscosity ν , the mass density ρ_f , a characteristic length (e.g. the integral length \bar{L} or the Taylor length $\bar{\lambda}$) and a characteristic velocity (e.g. the root mean square $\overline{u'}$ of fluctuation velocity). The parameters of particles are, on the other hand, the diameter D , the mass density ρ_p and the number N_p of particles. Therefore, there are four independent non-dimensional parameters. Here, we adopt $\overline{R_\lambda} = \overline{u'\lambda/\nu}$, the volume fraction Λ of the particles, the non-dimensional particle diameter D/\bar{L} and

	f	N^3	ν	\overline{R}_λ	L_0/\overline{L}	$\overline{L}/\overline{\eta}$	$\overline{\eta}/\Delta x$	CFL number
Run 256v	$f^{(v)}$	256^3	8×10^{-3}	48	5.3	48	1.0	6.4×10^{-2}
Run 512v	$f^{(v)}$	512^3					2.0	
Run 256i	$f^{(i)}$	256^3	7.13×10^{-3}	94	4.7	54	1.0	5.8×10^{-2}

Table 1: Parameters and statistics of single-phase turbulence. N^3 , number of grid points; L_0 ($= 2\pi$), side of the numerical domain; Δx ($= L_0/N$), grid width; ν , kinematic viscosity; R_λ , Taylor-length-based Reynolds number; L , integral length; η , Kolmogorov length. The CFL number is defined by the temporal average of $\sqrt{2K_t/3}\Delta t/\Delta x$ with the total kinetic energy K_t per unit mass and the time increment Δt of the temporal integration.

(a) Run 256v																
$D/\Delta x$	8	8	8	8	16	16	16	16	32	32	32	32	64	64	64	64
D/\overline{L}	0.17	0.17	0.17	0.17	0.33	0.33	0.33	0.33	0.66	0.66	0.66	0.66	1.3	1.3	1.3	1.3
γ	2	8	32	128	2	8	32	128	2	8	32	128	2	8	32	128
St	0.51	2.0	8.1	32	2.0	8.1	32	130	8.1	32	130	520	32	130	520	2100
N_p	512	512	512	512	64	64	64	64	8	8	8	8	1	1	1	1
N_L	202	202	202	202	805	805	805	805	3218	3218	3218	3218	12869	12869	12869	12869
Re_p	24	38	43	44	63	82	86	86	130	130	130	130	-	-	-	-

(b) Run 512v				
$D/\Delta x$	16	16	16	16
D/\overline{L}	0.17	0.17	0.17	0.17
γ	2	8	32	128
St	0.51	2.0	8.1	32
N_p	512	512	512	512
N_L	805	805	805	805

(c) Run 256i																
$D/\Delta x$	8	8	8	8	16	16	16	16	32	32	32	32	64	64	64	64
D/\overline{L}	0.15	0.15	0.15	0.15	0.29	0.29	0.29	0.29	0.59	0.59	0.59	0.59	1.2	1.2	1.2	1.2
γ	2	8	32	128	2	8	32	128	2	8	32	128	2	8	32	128
St	0.64	2.6	10	41	2.6	10	41	170	10	41	170	660	41	170	660	2700
N_p	512	512	512	512	64	64	64	64	8	8	8	8	1	1	1	1
N_L	202	202	202	202	805	805	805	805	3218	3218	3218	3218	12869	12869	12869	12869
Re_p	23	40	43	45	63	85	90	92	130	150	150	150	-	-	-	-

Table 2: Parameters of the particles: D , diameter; γ ($= \rho_p/\rho_f$), mass density ratio; St , Stokes number defined by T ; N_p , the number of particles; N_L , the number of force points on a particle. We use the values of \overline{L} and T of the single-phase turbulence (table 1). Note also that the volume fraction, Λ , is fixed to be 8.2×10^{-3} in all the cases. The particle Reynolds number, (3.3), is also listed in the last row of (a) and (c). We do not show Re_p for the largest particles because the relative velocity cannot be estimated.

the particle Stokes number $St = \tau_p/T$. Here,

$$\tau_p = \frac{\gamma D^2}{18\nu} \quad (\gamma = \rho_p/\rho_f) \quad (2.9)$$

is the relaxation time of particle velocity and $T = \overline{L}/\overline{u'}$ is the turnover time of the largest eddies. We conduct three series of DNS with fixed \overline{R}_λ and Λ ($= 8.2 \times 10^{-3}$) by changing D/\overline{L} and St ; see tables 1 and 2.

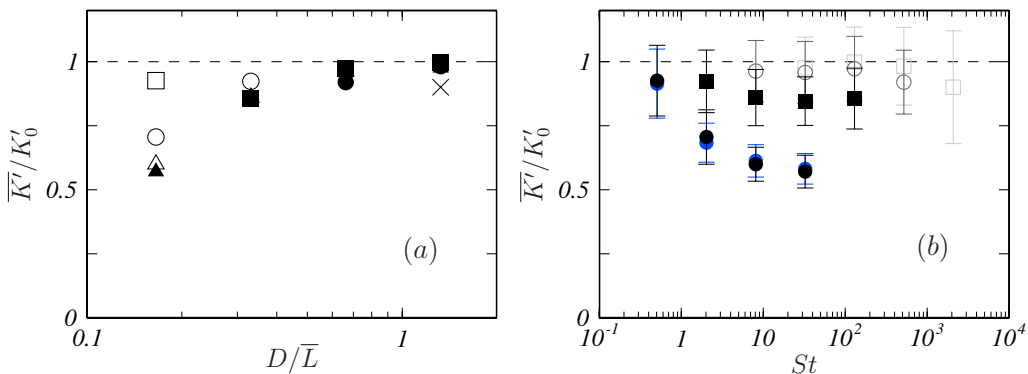


Figure 1: (a) Particle-size dependence of the temporal mean $\overline{K'}$ of the turbulent kinetic energy, which is normalized by the value K_0' for the single-phase flow. The results of Run 256v with forcing $\mathbf{f}^{(v)}$. Different symbols denote the results for different values of the Stokes number: $St = 0.51$, \square ; 2.0, \circ ; 8.1, \triangle ; 32, \blacktriangle ; 130, \blacksquare ; 520, \bullet ; 2100, \times . (b) Stokes-number dependence of $\overline{K'}$. Different symbols correspond to different particle diameters: $D/\overline{L} = 0.17$, \bullet ; 0.33, \blacksquare ; 0.66, \circ ; 1.3, \square . In the cases of the smallest particles ($D/\overline{L} = 0.17$), we also show the results of higher-resolution DNS (Run 512v) with blue symbols. Error bars indicate the standard deviation of $K'(t)$.

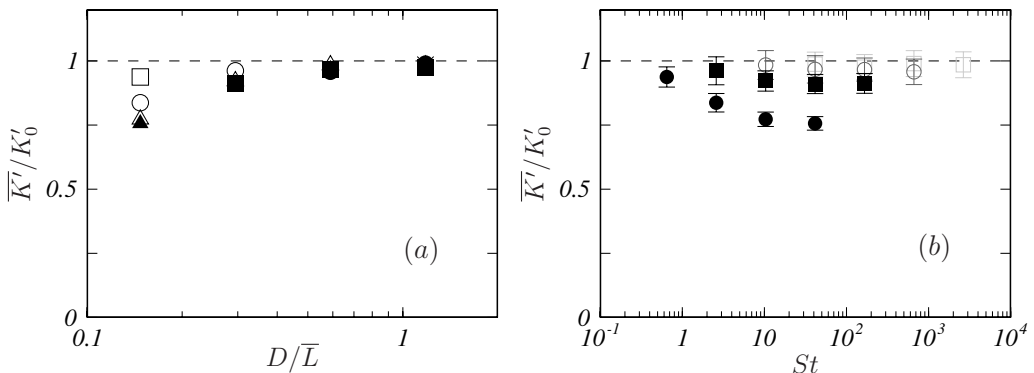


Figure 2: Same as figure 1 but for the other forcing $\mathbf{f}^{(i)}$ (Run 256i). (a) Different symbols denote the results with different values of the Stokes number: $St = 0.64$, \square ; 2.6, \circ ; 10, \triangle ; 41, \blacktriangle ; 170, \blacksquare ; 660, \bullet ; 2700, \times . (b) Different symbols correspond to different particle diameters: $D/\overline{L} = 0.15$, \bullet ; 0.29, \blacksquare ; 0.59, \circ ; 1.2, \square .

3. Results

The target of the present study is the attenuation of the turbulent kinetic energy defined by (2.6). First, we examine the turbulence driven by the external force $\mathbf{f}^{(v)}$. We show the temporal average $\overline{K'}$, normalized by the value K_0' for the single-phase flow, in figure 1(a) as a function of the particle diameter D normalized by the integral length \overline{L} . Here, we have evaluated $K'(t)$ as the spatial average of the turbulent kinetic energy of the fluid by using the method proposed by Kempe & Fröhlich (2012) to calculate the volume fraction of the fluid phase in each grid cell. It is clear, in figure 1(a), that $D \lesssim \overline{L}$ is a necessary condition for turbulence attenuation. This is consistent with the conventional view (Gore & Crowe 1989).

However, looking at the result with $D = 0.17\bar{L}$ and $St = 0.51$ for example, it is also clear that $D \lesssim \bar{L}$ is not the sufficient condition for the attenuation and that the degree of the turbulence reduction depends on the Stokes number.

The St -dependence of the attenuation rate is evident in figure 1(b). Looking at the case with the smallest particles $D = 0.17\bar{L}$ (• in figure 1b), we can see that the attenuation is more significant for larger St and it saturates for $St \gtrsim 10$, for which we observe about 43% reduction of \bar{K}' . Recall that the volume fraction Λ of the particles is only 8.2×10^{-3} . Although larger particles with $D = 0.33\bar{L}$ (■ in figure 1b) also attenuate the turbulence, the attenuation rate is smaller than the cases with $D = 0.17\bar{L}$. However, the tendency that the attenuation rate, for fixed D , is larger for larger St and it saturates for $St \gtrsim 10$ is common in the both cases with $D = 0.17\bar{L}$ and $0.33\bar{L}$. Larger particles with $D = 0.66\bar{L}$ or $1.3\bar{L}$ cannot attenuate turbulence even if $St \gg 1$.

To verify the numerical accuracy, we also show the results of Run 512v in figure 1(b). Recall that Runs 512v and 256v treat the common physical parameters (table 2) with different spatial resolutions for the smallest particles ($D = 0.17\bar{L}$), since it is particularly important to show that the significant reduction of turbulence intensity with those small particles is not an artifact. The results (blue symbols) with the higher resolution (Run 512v) and those (black ones) of Run 256v are in good agreement.

Next, we look at the results (figure 2) with the other forcing $\mathbf{f}^{(i)}$. The trend of the attenuation of turbulence driven by $\mathbf{f}^{(i)}$ is similar to the case with $\mathbf{f}^{(v)}$ shown in figure 1; the turbulence intensity is attenuated when $D \lesssim \bar{L}$ and the attenuation rate is larger for larger St for fixed D . We also notice that the attenuation rate of turbulence driven by $\mathbf{f}^{(i)}$ is smaller than the case with $\mathbf{f}^{(v)}$. This is due to the fact that there is no mean flow in turbulence driven by $\mathbf{f}^{(i)}$. We will discuss this difference below in more detail.

We have observed in figures 1 and 2 that, for fixed D , the attenuation is more significant for larger St and it saturates when $St \gtrsim 10$. We can explain these observations by the facts that (i) the relative velocity magnitude between a particle and surrounding fluid is determined by St , and (ii) it is an increasing function of St which tends to a value of $O(u')$ for $St \gg 1$. To demonstrate these facts, we plot in figure 3(a) the average relative velocity magnitude, $\overline{\langle |\Delta \mathbf{u}| \rangle}_p$, as a function of St for Run 256v. Here, $\langle \cdot \rangle_p$ denotes the average over particles and we evaluate $\Delta \mathbf{u}$ for each particle by using the method proposed by Kidanemariam *et al.* (2013) and Uhlmann & Chouippe (2017), where we define the velocity of the surrounding fluid of a particle by the average fluid velocity on the surface of the sphere with diameter $2D$ concentric with the particle. It is clear that the relative velocity magnitude tends to be a value of $O(u')$ when $St \gtrsim 10$ in the cases $D = 0.17\bar{L}$ (•) and $0.33\bar{L}$ (■). Note that for larger particles (e.g. the results shown in light gray for $D = 0.68\bar{L}$) the estimated values of $\Delta \mathbf{u}$ may have less meaning because these diameters are too large to define fluid velocity.

Similar dependence of $\overline{\langle |\Delta \mathbf{u}| \rangle}_p$ on St and D is observed in figure 3(c) for the case (Run 256i) with the other forcing $\mathbf{f}^{(i)}$. Looking at the results with $D = 0.15\bar{L}$ (•) and $0.29\bar{L}$ (■), we can see that the relative velocity magnitude is larger for larger St and it tends to a value for $St \gg 10$. It is clear in figures 3(a) and 3(c) that the velocity difference magnitude only weakly dependent on the particle size. This is reasonable because the Stokes number $St (= \tau_p/T)$ determines particles' ability

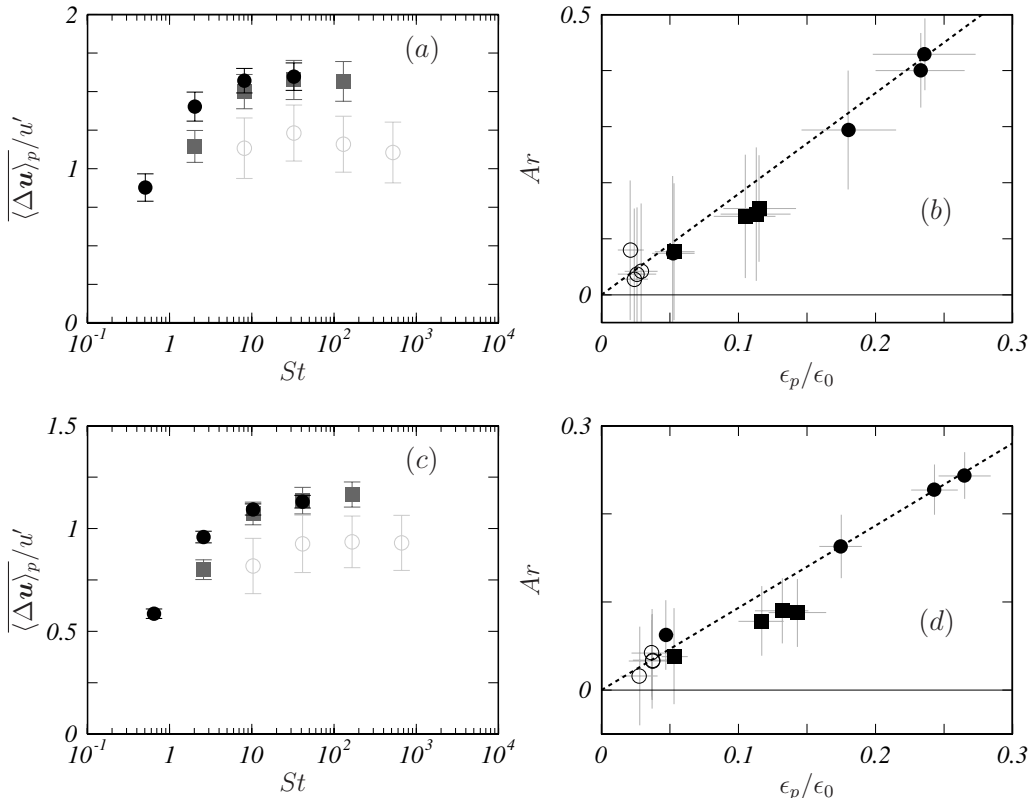


Figure 3: (a, c) Average relative velocity between a particle and the surrounding fluid. (b, d) Correlation between the attenuation rate (3.2) of the turbulent intensity and the estimate (3.1) of the energy dissipation rate ϵ_p due to particles normalized by the mean energy dissipation rate ϵ_0 of single-phase turbulence. For the estimation of ϵ_p , we put $C_p = 1$. The results for (a, b) Run 256v (with $\mathbf{f}^{(v)}$) and (c, d) Run 256i (with $\mathbf{f}^{(i)}$). Different symbols are the results for different particle diameters: (a, c) $D/\bar{L} = 0.17$, \bullet ; 0.33 , \blacksquare ; 0.66 , \circ ; (b, d) $D/L = 0.15$, \bullet ; 0.29 , \blacksquare ; 0.59 , \circ . The proportional coefficients of the dotted lines in (b) and (d) are 1.8 and 0.93, respectively. Error bars indicate the standard deviations of the temporal fluctuations.

to follow the swirling of the largest (i.e. most energetic) eddies. We also notice that the relative velocity magnitude normalized by u' is larger for $\mathbf{f}^{(v)}$ than $\mathbf{f}^{(i)}$. Since turbulence driven by $\mathbf{f}^{(v)}$ is accompanied by mean flow, the velocity of surrounding fluid, and therefore $|\Delta \mathbf{u}|$, can be larger.

Since we have computed the relative velocity, we can estimate the energy dissipation rate due to the shedding vortices around particles by

$$\epsilon_p = C_p \Lambda \frac{\overline{|\Delta \mathbf{u}|^3}_p}{D}. \quad (3.1)$$

Here, C_p is a constant of $O(1)$ and Λ is the volume fraction of the particles. Although the estimation of ϵ_p by (3.1) is an approximation because the drag coefficient, and therefore C_p , depend on the particle Reynolds number [see (3.3), below], this approximation is sufficient in the following arguments. The additional energy dissipation rate ϵ_p is the key quantity to understanding the turbulence attenuation. In fact, it is evident in figures 3(b) and 3(d) that the attenuation

rate defined by

$$Ar = \frac{K'_0 - \overline{K'}}{K'_0} \quad (3.2)$$

is approximately proportional to ϵ_p . This is the most important observation of the present DNS. Note that the proportional coefficient, $Ar/(\epsilon_p/\epsilon_0)$, is about twice larger for the turbulence driven by $\mathbf{f}^{(v)}$ than that by $\mathbf{f}^{(i)}$. We will show, in the next section, the origin of this difference [see (4.10)].

By using the estimated relative velocity magnitude, we can also estimate the particle Reynolds number

$$Re_p = \frac{D \langle |\Delta \mathbf{u}| \rangle_p}{\nu} \quad (3.3)$$

to verify that Re_p is sufficiently large for all the examined cases. The estimated values are listed in table 2. For example, for $St = 32$, $Re_p = 44$ (for $D = 0.17\overline{L}$), 86 (for $0.33\overline{L}$), 130 (for $0.66\overline{L}$). This means that vortices are shedding from the particles in these cases. It is, however, important to emphasize that although $Re_p \gg 1$ is a necessary condition for the turbulence attenuation, the large Re_p does not always imply a large attenuation rate, which depends on D .

4. Discussions

4.1. Condition for turbulence attenuation

On the basis of the DNS results, here we derive the condition for turbulence attenuation. Shedding vortices around particles are relevant to turbulence modulation. If they are larger than the largest eddies in single-phase turbulence, they enhance turbulent fluctuations, whereas shedding vortices smaller than the largest eddies can attenuate turbulence. Therefore,

$$D \lesssim L \quad (4.1)$$

is a necessary condition for the attenuation as proposed by Gore & Crowe (1989). For simplicity, in this section, we neglect the temporal fluctuations of $L(t)$, $\lambda(t)$ and $u'(t)$ and omit the over-bars of \overline{L} , $\overline{\lambda}$ and $\overline{u'}$. The DNS results shown in the previous section (see figures 3b and 3d) indicate that the attenuation rate is determined by the energy dissipation rate (3.1) due to shedding vortices. Therefore, turbulence attenuation requires, in addition to (4.1), the conditions for shedding vortices to acquire their energy from the turbulence: (i) there exists non-negligible (i.e. $\mathcal{O}(u')$) relative velocity between particles and their surrounding fluid and (ii) the particle Reynolds number (3.3) is high enough.

First, we examine (i), which is the condition for particles not to follow the surrounding flow. In other words, the particle velocity relaxation time τ_p is larger than the turnover time of the largest eddies: i.e. $St \gg 1$. Estimating τ_p by (2.9), we can express this condition ($St \gg 1$) as

$$D \gg \sqrt{\frac{18}{\gamma Re}} L \sim \frac{\lambda}{\sqrt{\gamma}}. \quad (4.2)$$

Here, we have defined the Reynolds number by $Re = u'L/\nu$ and used $T = L/u'$ and

the expression

$$\epsilon = \frac{15\nu u'^2}{\lambda^2} \sim \frac{u'^3}{L} \quad (4.3)$$

of the energy dissipation rate in isotropic turbulence (Taylor 1935).

Equation (4.2) implies that the sufficient velocity difference between particles and fluid requires that particle diameter D must be larger than a length proportional to the Taylor length λ . Note however that, when the mass density ratio γ is much larger than 1, particles smaller than λ can attenuate turbulence because of the coefficient $1/\sqrt{\gamma}$ on the right-hand side of (4.2). Indeed, this is the case for some parameters of the present DNS; for example, for Run 256v (see table 1) although $D = 0.17L$ is comparable with λ , St can be much larger than 1 when $\gamma \gg 1$, and in such cases turbulence is significantly attenuated (figure 1).

Next, we examine the second condition (ii). When (4.2) holds, the relative velocity magnitude is $O(u')$ (figures 3a and 3c), and therefore the particle Reynolds number (3.3) is $Re_p \approx u'D/\nu$. The condition for Re_p to be large is, therefore, expressed as

$$D \gg L/Re. \quad (4.4)$$

For $Re \gg 1$, if (4.2) holds, (4.4) also holds. Hence, (4.1) and (4.2) are the conditions for turbulence attenuation.

4.2. Estimation of attenuation rate

Further developing the above arguments, we may also estimate the attenuation rate of K' . Here, we assume that, if $D \ll L$, particles have only limited impact on the mean flow; this is indeed the case in the present system with mean flow driven by $\mathbf{f}^{(v)}$. Under this assumption, the energy input rate, $\langle \mathbf{U} \cdot \mathbf{f}^{(v)} \rangle$, is the same as in the single-phase turbulence. Hence, because of the statistical stationarity, the mean energy dissipation rate of the particulate turbulence is approximately equal to the value

$$\epsilon_0 = C_\epsilon \frac{(K_0 + K'_0)^{3/2}}{L} \quad (4.5)$$

for the single-phase flow. Here, $C_\epsilon (= O(1))$ is a flow-dependent constant (Goto & Vassilicos 2009), and K_0 and K'_0 denote the kinetic energy of the mean and fluctuating single-phase flow, respectively. Incidentally, in the turbulence driven by $\mathbf{f}^{(i)}$, although the mean flow is absent, the energy input rate is the same, by construction (2.4) of the forcing, in the single-phase and particulate flows.

In particulate turbulence with a small volume fraction of particles, the input energy is either transferred to the Kolmogorov scale by the energy cascading process from the forcing-scale eddies or dissipated in the wake behind particles. Hence, the energy dissipation rate is the sum of ϵ_c though the energy cascade and ϵ_p in the wake of the particles (i.e. the energy dissipation rate bypassing the energy cascade):

$$\epsilon_0 = \epsilon_c + \epsilon_p. \quad (4.6)$$

Here, ϵ_c is expressed by

$$\epsilon_c = C_\epsilon \frac{(K_0 + K')^{3/2}}{L} \quad (4.7)$$

in terms of the modulated turbulent kinetic energy K' . Then, substituting (4.5)

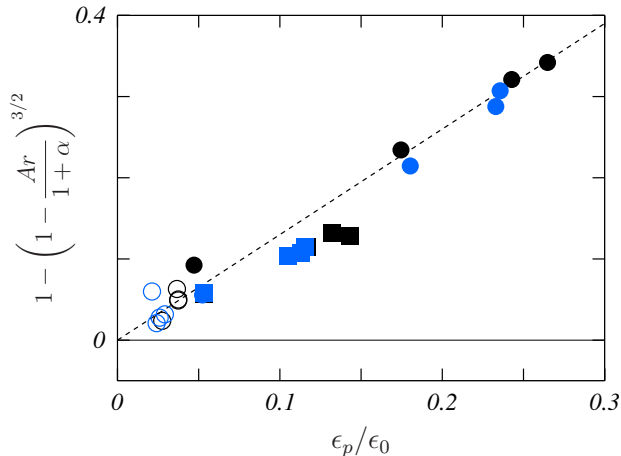


Figure 4: Verification of (4.8), according to which we replot the data in figures 3(b) and 3(d) with blue and black symbols, respectively. The dotted line indicates $1.3\epsilon_p/\epsilon_0$.

and (4.7) into (4.6) divided by ϵ_0 , we obtain the formula

$$1 - \left(1 - \frac{Ar}{1 + \alpha}\right)^{3/2} = \frac{\epsilon_p}{\epsilon_0} \quad (4.8)$$

for the attenuation rate Ar defined by (3.2). In (4.8), α denotes the ratio

$$\alpha = \frac{K_0}{K'_0} \quad (4.9)$$

between the mean and fluctuation energy of single-phase flow: $\alpha = 0$ for the turbulence driven by $\mathbf{f}^{(i)}$, whereas α is numerically estimated as 1.86/1.89 \approx 0.98 for $\mathbf{f}^{(v)}$. Note that although C_ϵ in (4.5) and (4.7) depends on flow, (4.8) is independent of C_ϵ . This means that the formula (4.8) is flow-independent. In fact, by using (4.8), the two data sets of Ar in figures 3(b) and 3(d) for the two kinds of forcing collapse (figure 4). The formula (4.8) further reduces to

$$Ar \sim \frac{(1 + \alpha) \epsilon_p}{\epsilon_0} \quad (4.10)$$

when Ar is not too large. This explains the reason why the proportional constant, $Ar/(\epsilon_p/\epsilon_0)$, figure 3(b), is approximately twice larger than that in figure 3(d). Recall that $\alpha + 1 \approx 1.98$ for $\mathbf{f}^{(v)}$ and $\alpha + 1 = 1$ for $\mathbf{f}^{(i)}$.

We emphasize that (4.8) can predict the attenuation rate Ar , if we know ϵ_p . By using (3.1), we may estimate ϵ_p for $St \gg 1$ because $|\Delta \mathbf{u}| = c u'$ for $St \gg 1$ with a flow-dependent constant c (figures 3a and 3c). Then, we may rewrite (4.8) as

$$1 - \left(1 - \frac{A}{1 + \alpha}\right)^{3/2} = \frac{C'_p \Lambda L}{D} \quad (St \gg 1). \quad (4.11)$$

Here, $C'_p \sim c^3 C_p / C_\epsilon$ is also a flow-dependent constant. The above equation may reduce to

$$Ar \sim \frac{(1 + \alpha) \Lambda L}{D} \quad (St \gg 1) \quad (4.12)$$

when Ar is not too large. This simple expression (4.12) explains that the attenu-

ation occurs when (4.1) holds with a sufficient volume fraction Λ . It also explains that the attenuation rate Ar is larger for smaller D . Hence, combining this with the condition (4.2), we conclude that particles with the size proportional to $\lambda/\sqrt{\gamma}$ most effectively attenuate turbulence intensity.

5. Conclusions

We have derived the conditions (4.1) and (4.2) for the dilute additives of solid spherical particles, without the gravity, to attenuate turbulence in a periodic cube. First, we have numerically verified the conventional picture that the attenuation is due to the additional energy dissipation rate ϵ_p , (3.1), caused by shedding vortices around particles; more concretely, we have shown in figures 3(b) and 3(d) that the attenuation rate Ar is approximately proportional to ϵ_p . This result immediately leads to the attenuation condition because the attenuation occurs when ϵ_p , (3.1), takes a finite value, which requires a finite relative velocity $|\Delta\mathbf{u}|$ between particles and their surrounding fluid; i.e. $St \gg 1$. In fact, as shown in figures 3(a) and 3(c), $|\Delta\mathbf{u}|$ takes finite values when $St \gtrsim 1$ and it tends to a value of $O(u')$ for $St \gtrsim 10$. The condition, $St \gg 1$, leads to (4.2) for the particle diameter D ; and if (4.2) holds, then $Re_p \gg 1$ and therefore vortices are shedding from the particles. Hence, (4.2) gives the lower bound of D for the turbulence attenuation. When (4.2) holds and $D > \bar{L}$, the shedding vortices enhance the turbulence. Therefore, (4.1), i.e. $D \lesssim \bar{L}$, gives the upper bound for the turbulence attenuation.

The picture of the turbulence attenuation due to the shedding vortices also leads to the estimation of the attenuation rate. The simple argument developed in §4.2 leads to (4.8), which well explains the DNS results (figure 4). We emphasize that (4.8) is a formula independent of forcing schemes. For $St \gg 1$, (4.8) reduces to (4.12), which implies that, for a given volume fraction, smaller particles which satisfy (4.2) more effectively attenuate turbulence. This is consistent with the DNS results (figures 1 and 2). Hence, we conclude that, in turbulence at sufficiently high Re (and therefore $L \gg \lambda \gg \eta$), particles with a size proportional to $\lambda/\sqrt{\gamma}$, where $\gamma = \rho_p/\rho_p$, most significantly attenuate turbulence.

Before closing this article, it is worth mentioning the possibility that particles can modulate turbulence even if they do not satisfy (4.2) because they can interrupt energy cascade in the inertial range. More concretely, if particles' velocity relaxation time τ_p is comparable with the turnover time $\tau(\ell)$ of eddies with size ℓ in the inertial range, they follow slow motion of eddies larger than ℓ , but they have relative velocity with those smaller than ℓ . Since larger eddies have more energy, the relative velocity between particles and fluid is determined by the eddies with size ℓ . Therefore, the particles acquire their energy from such eddies with size ℓ and the some part of energy cascade at scales smaller than ℓ may be bypassed by the shedding vortices behind particles and dissipated in the wake of particles. Such a phenomenon is to be numerically observed in turbulence at higher Reynolds numbers in the near future.

Acknowledgements. The DNS were conducted under the supports of the NIFS Collaboration Research Program (20KNSS145) and under the supercomputer Fugaku provided by RIKEN through the HPCI System Research projects (hp210207).

Funding. This study was partly supported by JSPS Grant-in-Aids for Scientific Research (20H02068).

Declaration of interests. The authors report no conflict of interest.

Author ORCIDs.

Sunao Oka <https://orcid.org/0000-0001-6398-9213>Susumu Goto <https://orcid.org/0000-0001-7013-7967>.

REFERENCES

- BURTON, T. M. & EATON, J. K. 2005 Fully resolved simulations of particle-turbulence interaction. *J. Fluid Mech.* **545**, 67–111.
- CISSE, M., SAW, E.-W., GIBERT, M., BODENSCHATZ, E. & BEC, J. 2015 Turbulence attenuation by large neutrally buoyant particles. *Phys. Fluids* **27**, 061702.
- COSTA, P., PICANO, F., BRANDT, L. & BREUGEM, W.-P. 2016 Universal scaling laws for dense particle suspensions in turbulent wall-bounded flows. *Phys. Rev. Lett.* **117**, 134501.
- COSTA, P., PICANO, F., BRANDT, L. & BREUGEM, W.-P. 2018 Effects of the finite particle size in turbulent wall-bounded flows of dense suspensions. *J. Fluid Mech.* **843**, 450–478.
- CROWE, C. T., TROUTT, T. R. & CHUNG, J. N. 1996 Numerical models for two-phase turbulent flows. *Ann. Rev. Fluid Mech.* **28**, 11–43.
- ELGHOBASHI, S. 1994 On predicting particle-laden turbulent flows. *Appl. Sci. Res.* **52**, 309–329.
- ELGHOBASHI, S. & TRUESDELL, G. C. 1993 On the two-way interaction between homogeneous turbulence and dispersed solid particles. i: Turbulence modification. *Phys. Fluids A* **5**, 1790–1801.
- FERRANTE, A. & ELGHOBASHI, S. 2003 On the physical mechanisms of two-way coupling in particle-laden isotropic turbulence. *Phys. Fluids* **15**, 315–329.
- FORNARI, W., FORMENTI, A., PICANO, F. & BRANDT, L. 2016 The effect of particle density in turbulent channel flow laden with finite size particles in semi-dilute conditions. *Phys. Fluids* **28**, 033301.
- GAO, H., LI, H. & WANG, L.-P. 2013 Lattice boltzmann simulation of turbulent flow laden with finite-size particles. *Comp. Math. Appl.* **65**, 194–210.
- GORE, R. A. & CROWE, C. T. 1989 Effect of particle size on modulating turbulent intensity. *Int. J. Multiphase Flow* **15**, 279–285.
- GOTO, S., SAITO, Y. & KAWAHARA, G. 2017 Hierarchy of antiparallel vortex tubes in spatially periodic turbulence at high reynolds numbers. *Phys. Rev. Fluids* **2**, 064603.
- GOTO, S. & VASSILICOS, J. C. 2009 The dissipation rate coefficient of turbulence is not universal and depends on the internal stagnation point structure. *Phys. Fluids* **21**, 035104.
- HOMANN, H. & BEC, J. 2010 Finite-size effects in the dynamics of neutrally buoyant particles in turbulent flow. *J. Fluid Mech.* **651**, 81–91.
- HOQUE, M. M., MITRA, S., SATHE, M. J., JOSHI, J. B. & EVANS, G. M. 2016 Experimental investigation on modulation of homogeneous and isotropic turbulence in the presence of single particle using time-resolved piv. *Chem. Eng. Sci.* **153**, 308–329.
- KAJISHIMA, T., TAKIGUCHI, S., HAMASAKI, H. & MIYAKE, Y. 2001 Turbulence structure of particle-laden flow in a vertical plane channel due to vortex shedding. *JSME Int. J. Ser. B* **44**, 526–535.
- KEMPE, T. & FRÖHLICH, J. 2012 An improved immersed boundary method with direct forcing for the simulation of particle laden flows. *J. Comp. Phys.* **231**, 3663–3684.
- KIDANEMARIAM, A. G., CHAN-BRAUN, C., DOYCHEV, T. & UHLMANN, M. 2013 Direct numerical simulation of horizontal open channel flow with finite-size, heavy particles at low solid volume fraction. *New J. Phys.* **15**, 025031.
- LAMORGESE, A. G., CAUGHEY, D. A. & POPE, S. B. 2005 Direct numerical simulation of homogeneous turbulence with hyperviscosity. *Phys. Fluids A* **17**, 015106.
- LIN, Z., YU, Z., SHAO, X. & WANG, L.-P. 2017 Effects of finite-size neutrally buoyant particles on the turbulent flows in a square duct. *Phys. Fluids* **29**, 103304.
- LUCCI, F., FERRANTE, A. & ELGHOBASHI, S. 2010 Modulation of isotropic turbulence by particles of taylor length-scale size. *J. Fluid Mech.* **650**, 5–55.
- LUCCI, F., FERRANTE, A. & ELGHOBASHI, S. 2011 Is stokes number an appropriate indicator for turbulence modulation by particles of taylor-length-scale size? *Phys. Fluids* **23**, 025101.
- MAXEY, M. & RILEY, J. 1983 Equation of motion of a small rigid sphere in a nonuniform flow. *Phys. Fluids* **26**, 883–889.

- PENG, C., AYALA, O. M. & WANG, L.-P. 2019 A direct numerical investigation of two-way interactions in a particle-laden turbulent channel flow. *J. Fluid Mech.* **875**, 1096–1144.
- PENG, C. & WANG, L.-P. 2019 Direct numerical simulations of turbulent pipe flow laden with finite-size neutrally buoyant particles at low flow reynolds number. *Acta Mechanica* **230**, 517–539.
- PICANO, F., BREUGEM, W.-P. & BRANDT, L. 2015 Turbulent channel flow of dense suspensions of neutrally buoyant spheres. *J. Fluid Mech.* **764**, 463–487.
- SAFF, E. B. & KUIJLAARS, A. B. J. 1997 Distributing many points on a sphere. *Math. Intell.* **19**, 5–11.
- SCHNEIDERS, L., MEINKE, M. & SCHRÖDER, W. 2017 Direct particle-fluid simulation of kolmogorov-length-scale size particles in decaying isotropic turbulence. *J. Fluid Mech.* **819**, 188–227.
- SHAO, X., WU, T. & YU, Z. 2012 Fully resolved numerical simulation of particle-laden turbulent flow in a horizontal channel at a low reynolds number. *J. Fluid Mech.* **693**, 319–344.
- TAYLOR, G. I. 1935 Statistical theory of turbulence. *Proc. Roy. Soc. A* **151**, 421–444.
- TEN CATE, A., DERKSEN, J. J., PORTELA, L. M. & AKKER, H. E. A. VAN DEN 2004 Fully resolved simulations of colliding monodisperse spheres in forced isotropic turbulence. *J. Fluid Mech.* **519**, 233–271.
- TSUJI, Y. & MORIKAWA, Y. 1982 LDV measurements of an air–solid two–phase flow in a horizontal pipe. *J. Fluid Mech.* **120**, 385–409.
- TSUJI, Y., MORIKAWA, Y. & SHIOMI, H. 1984 LDV measurements of an air–solid two–phase flow in a vertical pipe. *J. Fluid Mech.* **139**, 417–434.
- UHLMANN, M. 2005 An immersed boundary method with direct forcing for the simulation of particulate flows. *J. Comp. Phys.* **209**, 448–476.
- UHLMANN, M. 2008 Interface-resolved direct numerical simulation of vertical particulate channel flow in the turbulent regime. *Phys. Fluids* **20**, 053305.
- UHLMANN, M. & CHOUippe, A. 2017 Clustering and preferential concentration of finite-size particles in forced homogeneous-isotropic turbulence. *J. Fluid Mech.* **812**, 991–1023.
- WANG, G., ABBAS, M. & CLIMENT, É. 2017 Modulation of large-scale structures by neutrally buoyant and inertial finite-size particles in turbulent couette flow. *Phys. Rev. Fluids* **2**, 084302.
- WANG, L.-P., PENG, C., GUO, Z. & YU, Z. 2016 Flow modulation by finite-size neutrally buoyant particles in a turbulent channel flow. *J. Fluids Eng.* **138**, 041306.